Airborne Retrievals of Snow and Ice Surface Emissivity at Millimeter Wavelengths

Tim J. Hewison, *Member, IEEE,* and Stephen J. English

***Abstract*—Passive microwave radiometers (24–157 GHz) have been flown over Baltic sea ice and snow sites in April 1995 and on March 15, 1997. Data from these instruments are analyzed with reference to ground measurements of snow and ice conditions, and emissivity spectra are presented for 12 classifications of surface type. A simple model based on dielectric permittivity can accurately represent the microwave spectra of sea ice, but cannot be extended to the behavior of dry snow above 100 GHz without the addition of an extra term to represent volume scattering. The parameterization presented is intended to provide a background for temperature and humidity retrievals from satellite sounders, but the results will be of interest to the snow and ice remote-sensing communities.**

***Index Terms*— Microwave radiometry, millimeter wave radiometry, sea ice, snow, surfaces.**

I. Introduction

SUCCESSFUL use of satellite microwave radiometer data for temperature and humidity retrievals in numerical weather prediction requires that emission and scattering by the surface be parameterized in a realistic way in the radiative transfer model. This paper presents airborne measurements over snow and ice surfaces, and a simple model capable of describing how the microwave emissivity varies with frequency, polarization, and incidence angle. This model is intended to supply a background emissivity for retrievals over various categories of surface.

MACSI (microwave airborne campaign over snow and ice) took place from March 30 to April 6, 1995. It was the follow-up to SAAMEX (Surface and Aircraft Microwave Experiment) [1] of March 1990, which was conducted over the same area, with a more limited range of microwave measurements and generally wetter snow conditions.

The main part of the experiment was conducted over fixed ground sites, arranged in two lines. There were four ice sites in the northern Baltic Sea (Gulf of Bothnia), and four snow sites over Finland, inland of Oulu. The sites are shown in Fig. 1.

The intention of MACSI was to measure sea ice and snow during the spring, when climatologically the ice extent is at its maximum, and snow conditions were expected to change from wet at Oulu to dry in the hills near Pudasjärvi. However, the southern sea ice edge was well to the north of the expected position, so Ice Site 1 was mostly open water. Snow conditions were as expected, with deep, dry snow in the hills, but shallower, wet snow over the sea ice and at the low-altitude snow sites.

Manuscript received August 13, 1997; revised June 24, 1998.

The authors are with the Remote Sensing Branch, U.K. Meteorological Office, DERA Farnborough, Hants., GU14 0LX, U.K. (e-mail: tjhewison@meto.gov.uk).

Publisher Item Identifier S 0196-2892(99)03486-5.

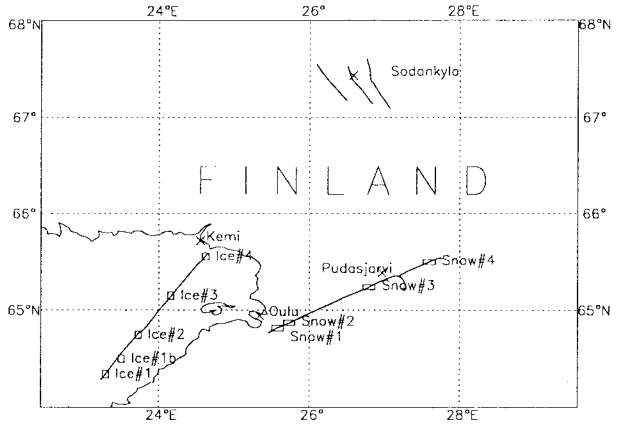

Fig. 1. Map of test sites, weather stations, and aircraft tracks.

More recently, on March 15, 1997, the Baltic sea ice was revisited, and Sodankylä, in northern Finland, was overflown to sample dry snow over a forested site, as part of the WINTEX experiment (land–surface–atmosphere interactions in a wintertime boreal landscape).

A. Past Measurements and Modeling

Physical modeling of sea ice and snow requires sophisticated techniques. Tsang *et al.* [2] show that the real part of the relative permittivity of sea ice is about 3.2, and the imaginary part varies from 10^{-4} to 0.05. New ice has few inhomogeneities, and can be modeled as an incoherent dielectric slab [3] between air and saline water. As the slab thickens, its emission increases from that of open water to a saturation value (0.93–0.98), which occurs at 10 mm for 90 GHz and 20 mm at 18.7 GHz [4].

As ice ages, more brine and air pockets form, which act as volume scatterers, decreasing the emissivity at higher frequency. The Maxwell-Garnett [5] mixing theory provides the effective permittivity of a distribution of dielectric spheres, but does not allow for volume scattering, and thus a dielectric model using the Maxwell-Garnett theory is only appropriate for low frequencies. At microwave frequencies, dense medium theory [2] or strong fluctuation theory [6] can be used to account for the interaction between the scatterers.

Dry snow has a real relative permittivity of 1.2–2.8, with an imaginary part varying from 10^{-4} to 10^{-2} [3]. As dry snow ages, its emissivity decreases as the grains which act as

volume scatterers increase in size, and can be represented in a similar way to old ice. The spectral dependence on grain size of a dry snow pack was observed by Lohanick [7] and Sherjal *et al.* [8]. Wet snow has a much larger permittivity, due to the ice particles' coating of liquid water, which makes it almost a microwave black body.

At low frequency, where the penetration depth is high, the interaction with the snow pack is small, and the interface between the snow and the underlying surface is important [9]. Conversely, at higher frequency, penetration depths become small, and the emissivity depends on the snow pack age, wetness, and surface state (e.g., refrozen, fresh, wet).

The SAAMEX experiment [1] provided measurements at 89 and 157 GHz, which at times showed quite different behavior from lower frequency measurements. In this paper, we present an extensive set of measurements at 157 GHz, alongside lower frequency measurements allowing comparison with past results. Emissivity at these high frequencies is very important for humidity sounding and temperature sounding in cloudy regions, as the ability of instruments like the AMSU-B (advanced microwave sounding unit) to detect and correct errors in humidity fields depends very strongly on the value of emissivity and on the error in the emissivity model [10].

II. Proposed Model

Given the limited information available for modeling the sea ice and snow on a scale appropriate for satellite retrievals, a fully physical model is not feasible. In a typical retrieval scheme, a simple model is required to provide an initial best guess for the emissivity of various surface categories. Iterative solution then finds temperature and humidity profiles and emissivity coefficients most consistent with satellite radiances.

In this paper, a semiempirical model is presented for the emissivity of the ice/snowpack/forest canopy system as a whole. In this way, the surface can be represented in terms of a specular reflector, based on a Debye-like form of effective relative permittivity ε at frequency ν, which is parameterized in terms of ε_s, the effective static permittivity ε_∞, its high-frequency limit, and ν_r, the effective relaxation frequency. The ionic conductivity term has been neglected, as its contribution is insignificant above 20 GHz.

$$\varepsilon(\nu) = \frac{\varepsilon_s - \varepsilon_\infty}{1 - i \cdot \nu/\nu_r} + \varepsilon_\infty. \tag{1}$$

The Fresnel formulas, below, define the power reflectivity in vertical and horizontal polarizations Γ_v and Γ_h of a specular surface in terms of its complex relative permittivity ε and the angle of incidence θ. The emissivity (ϵ) is the complement of this [$\epsilon(\nu, \theta) = 1 - \Gamma(\nu, \theta)$].

$$\Gamma_v(\nu, \theta) = \left| \frac{-\varepsilon(\nu)\cos\theta + \sqrt{\varepsilon(\nu) - \sin^2\theta}}{\varepsilon(\nu)\cos\theta + \sqrt{\varepsilon(\nu) - \sin^2\theta}} \right|^2$$

or

$$\Gamma_h(\nu, \theta) = \left| \frac{\cos\theta - \sqrt{\varepsilon(\nu) - \sin^2\theta}}{\cos\theta + \sqrt{\varepsilon(\nu) - \sin^2\theta}} \right|^2. \tag{2}$$

Such a scheme can represent dielectric surfaces, such as open water, by setting $\varepsilon_s > \varepsilon_\infty$, and volume scattering, such as sea ice, by $\varepsilon_s < \varepsilon_\infty$. However, surfaces exhibiting nonmonotonic emissivity spectra cannot be accurately presented without the addition of a scattering term. It is proposed that the effects of various forms of snow and vegetation cover are absorbed into these three parameters.

Bragg scattering by small-scale surface roughness was modeled by Choudhury *et al.* [11] by scaling the surface reflectivity by an exponential factor of a roughness parameter $h' = (4\pi\nu\sigma/c)^2$, where σ is the rms height of the surface

$$\epsilon_p(\nu, \theta) = 1 - \Gamma_p(\nu, \theta) e^{-h' \cos^2\theta}. \tag{3}$$

However, such a formulation takes no account of the fact that the surface correlation length is typically much larger than the rms roughness when measured at a scale appropriate for millimeter wavelengths. To allow for this, roughness is often regarded as a free parameter for a given surface, independent of frequency. In the model proposed in this paper, such roughness is simply absorbed into the effective permittivities.

Geometric optics can be used to give a more realistic representation of surface roughness by calculating the reflectivity for a myriad of surface facets. However, the integration over the distribution of facets renders this approach too computationally expensive for use in operational retrievals.

An additional parameter for polarization mixing, Q, was added by Wang and Choudhury [12], and is included in the proposed model to explain the observed angular variation of emissivity:

$$\Gamma'_h = (1 - Q)\Gamma_h + Q\Gamma_v$$

or

$$\Gamma'_v = (1 - Q)\Gamma_v + Q\Gamma_h. \tag{4}$$

Most vegetation and very deep, dry snow appear optically thick at millimeter wavelengths due to absorption and volume scattering. This process is absorbed into the effective permittivities and setting the polarization-mixing parameter $Q = 0.5$ in the proposed model. The effective surface temperature is that of the snow or vegetation, as measured by thermal infrared radiometry.

III. Measurements

A. Instrumentation

This paper presents measurements made by the U.K. Meteorological Office (UKMO) on the C-130 Hercules. The key instruments flown for this experiment were microwave radiometers, known as Deimos and MARSS (microwave airborne radiometer scanning system). These are total power radiometers, both with a 3 s along-track scan, which includes various views downward (and upward for MARSS) and two onboard black body calibration targets. Table I summarizes their performance during MACSI and WINTEX. These instruments are described in full in [13], [14].

The UKMO aircraft also operated a range of meteorological and navigational instrumentation, useful to the analysis

TABLE I
SUMMARY OF UKMO MICROWAVE AIRBORNE RADIOMETER SYSTEMS

Instrument	Deimos		MARSS	
Frequency /GHz	23.8	50.1	89.0	157.0
View angle	+35° to -5° Down only		+40° to -40° Up and Down	
Scan period	3s		3s	
Beamwidth (3dB)	11°		10°	
Polarisation MACSI	Mixed	Mixed	Mixed	V or H
Polarisation WINTEX	V,H	V,H	Mixed	V or H
Integration time	50ms	50ms	80ms	80ms
Sensitivity, ΔT	0.6K	0.6K	0.3K	0.5K
Absolute Accuracy	1.4K	1.7K	1.1K	1.0K

TABLE II
MARCH 1997 WEATHER OBSERVATIONS AT SODANKYLÄ

Date	UTC	T_{MAX}	T_{MIN}	Snow Depth
12/3/97	0600	1.5°C	-4.6°C	86cm
12/3/97	1800	-0.4°C	-5.1°C	86cm
13/3/97	0600	-5.0°C	-12.7°C	87cm
13/3/97	1800	-1.6°C	-6.2°C	96cm
14/3/97	0600	-4.5°C	-11.0°C	96cm
14/3/97	1800	-4.9°C	-14.6°C	93cm
15/3/97	0600	-12.9°C	-29.0°C	92cm
15/3/97	1800	-5.2°C	-28.5°C	91cm

of the data, including air temperature, humidity, pressure, wind speed, surface temperature (from a thermal infrared radiometer) and albedo (from upper and lower hemispherical pyranometers), GPS position, and radar altitude. However, the most useful instrument for identification of surface conditions was the downward-facing video camera.

On April 4 and 5, 1995, Helsinki University of Technology (HUT) operated several microwave radiometers (6.8, 10.7, 18.7, and 24.0 GHz) on their "Skyvan" aircraft over all of the test sites. Data from these radiometers have been compared with the UKMO instruments [15], but have not been included in this analysis.

B. Flights

The UKMO C-130 overflew the test sites on five days from March 30 to April 5, 1995. These flights consisted of straight runs at low level (160–1200 m) over the test sites and profiles from 16–7600 m for radiative transfer modeling. Also, ridged ice was overflown in eight directions to determine the dependence of emissivity on the ridge orientation. A sortie was also made over the Barents Sea, near Svalbard, on April 7, 1995 to sample arctic ice types. These flights are described in full in [17].

Additional measurements were made as part of another campaign, WINTEX, on March 15, 1997. This included low-level runs over the sea ice in the Gulf of Bothnia on route to the experimental site, at Sodankylä, where three tracks were flown at various altitudes from 76 to 1200 m over partially forested areas with deep, dry snow cover.

C. Ground Truth

For MACSI, ground truth measurements of snow and ice thickness, density, and water content were made at each of the fixed sites, shown in Fig. 1. More details are given in [16].

During the period March 31–April 6, 1995, the Finnish research vessel Aranda was positioned just north of Ice Site 3, at a position known as "3b." This was used as a base for the ground truth measurements at Ice Sites 2, 3, 3b, and 4. These comprised ice thickness, salinity and temperature profiles, and snowfork measurements of snow depth, density, wetness, and temperature profiles.

Some ice roughness measurements were also made near Aranda using a laser distance meter. These indicated a small-scale surface roughness (rms height) of approximately 2 mm and correlation lengths 10–80 mm. Thus, compact consolidated ice surfaces can be considered very rough at millimeter wavelengths. Thin new ice, such as nilas, was not measurable with this system, but was observed to be very flat.

Although a range of ice types was experienced, the ground sites were dominated by compact consolidated ice. The ice thickness increased from nil at Site 1 to 60 cm at Site 4. Snow cover was variable, typically 20 cm deep of volumetric moisture (m_v) between 0.0 and 0.4% and density increasing from 200 kg/m^3 at the surface to 400 kg/m^3 nearer the ice.

The snow sites were sampled at 1 km intervals within 3 h of the flight times. In addition to snow depth, snowfork measurements of wetness and density profiles were taken along the center line of each snow site. The wetness figures quoted in this paper are the maximum value to volumetric moisture (m_v) in the top 10 cm of snow, averaged over each test site. The samples were found to be highly variable in depth and position, complicating interpretation of aircraft data.

Snow Site 1 was agricultural, mostly open fields with about 6 cm of usually wet ($m_v \approx 0.5\%$) snow. The other snow sites were more forested, each showing 40% vegetation cover above the snow, as viewed from the aircraft. No snow was present on the trees. Average snow depths of 43, 65, and 92 cm were recorded for Sites 2, 3, and 4, respectively. However, the wetness and density of the snow pack were highly variable through its depth, along each site and from day to day.

Weather data were available from a number of sources [16]. Analysis charts of the synoptic situation show that an occlusion passed through the area on April 1, producing a few centimeters of fresh snowfall. Four temporary weather stations recorded meteorological data at half-hourly intervals throughout the experiment at Ice Site 4 and Snow Sites 2, 3, and 4. Three hourly observations from Ulkokalla, Marjaniemi, Hailuoto, Kemi1, Oulu, and Pudasjärvi[1] showed that daily air temperatures rose close to 0°C throughout MACSI which, with direct solar heating, was enough to cause melting on the surface.

No ground data are available for March 15, 1997. However, the synoptic situation over Finland had just changed from a mild southwesterly flow to a cold northerly one. 10 cm of fresh snow fell on March 13, and temperatures fell from +1.5°C on March 12 to −29°C. The snow was deep and dry on the day of the flight. Table II summarizes the maximum and minimum air temperature and snow depth at Sodankylä at 12-h intervals throughout the period. During this period, extensive areas of

[1] Supplied by the Finnish Meteorological Institute (FMI).

new ice formed in the Baltic Sea, with localized cover of thin, dry snow.

IV. Emissivity Calculation

Measured brightness temperatures must be converted to surface emissivity to extend them to general application. The following formula is used to calculate the emissivity using only aircraft data:

$$\epsilon(\nu, \theta) = \frac{T_n(\nu, \theta) - T_z(\nu, \theta)}{T_s - T_z(\nu, \theta)} \tag{5}$$

where ϵ is the emissivity at frequency ν and incidence angle θ, T_n, and T_z are the up- and downwelling brightness temperatures, respectively, and T_s is the surface (skin) temperature. The calculation of each of these terms is discussed below.

This emissivity calculation assumes surface reflection to be purely specular, as this is consistent with the treatment used for the sea surface in fast radiative transfer models, e.g., RTTOV [18]. However, most surfaces observed during MACSI were close to Lambertian. The absolute accuracy of this emissivity calculation is calculated to be 0.006 for $\epsilon = 0.900$. This is dominated by uncertainty in absolute brightness temperatures.

A. Predict Downwelling Brightness Temperatures

Downwelling brightness temperatures T_z at Deimos frequencies are not directly measured, but can be predicted from MARSS' observations. Liebe's [19] radiative transfer model has been applied to calculate T_z at Deimos and MARSS frequencies for 1200 example atmospheres. Coefficients have been produced by multiple linear regression of T_z at 89 and 157 GHz to predict T_z at 24 and 50 GHz at 17 vertical levels. These predictions are accurate to within 1.2K under clear skies, where the atmospheric emission is only dependent on water vapor and oxygen species. It is less accurate ($\approx$5K) in cloudy conditions, due to the additional scattering.

B. Translate to Specular View Angle

To calculate the emissivity of a specular surface, T_z must be translated to the same angle as the downward view T_n by scaling by $\sec(\theta)$ to calculate the emissivity, approximating the atmosphere to be plane, parallel, and optically thin.

C. Correct for Atmospheric Absorption

The atmosphere below the aircraft will affect the measured brightness temperatures by absorption and emission (scattering is neglected, as there must be no cloud below the aircraft for surface observation). The optical depth of this slab of atmosphere must be estimated so a correction can be applied to compensate for this effect. Radiative transfer models (Liebe [19] for microwave, MODTRAN [20] for infrared) were used to calculate the transmissivity of 1200 example atmospheres between 950–1000 hPa. Coefficients of air temperature and humidity mass mixing ratio at 950 hPa have been produced by multiple linear regression to predict the transmissivity of this slab. Thus, the optical depth from 950 to 1000 hPa can be predicted from the temperature and humidity at the flight level, and this is then scaled by the atmospheric path length to produce the transmissivity. Corrections to the measured brightness temperatures, both up- and downwelling microwave and infrared are then calculated, assuming an effective radiative temperature equal to the average of that at the flight level and the ground. These corrections are very small (<1K) for most arctic atmospheres at 300 m flight altitude.

D. Infrared Emissivity Correction

Strictly, allowance should be made for surfaces with an infrared emissivity of less than 1. This will introduce a bias in the measurement of surface temperature which, in turn, will bias the resultant microwave emissivity. No consistent figures for the emissivity of snow surfaces in the thermal infrared were available in the literature, so no correction has been applied, resulting in a microwave emissivity, relative to that of the thermal infrared. However, the worst case is expected to be for bare new ice, with an emissivity $\epsilon^{\mathrm{ir}} = 0.96$ in the thermal infrared [21], in clear arctic skies ($T_z^{\mathrm{ir}} = 211$K); this causes the surface temperature to be underestimated by 2.4K which, in turn, overestimates the microwave emissivity of $\epsilon = 0.920$ by approximately 0.010, depending on the downwelling brightness temperature.

V. Nadir Emissivity Spectra

Footage from the aircraft's downward facing video camera was studied to identify periods during which homogeneous surface types were overflown, known as "samples." A category was assigned to each sample, which ranged from 9 to 140 s, corresponding to track lengths of 800 m–13 km.

The emissivity was calculated for each second within a sample as described in Section IV, and samples of similar surface categories were then combined to produce nadir emissivity spectra. Effective permittivity and roughness parameters (ε_s, ε_∞, ν_r, σ) for the proposed model were then calculated as a least squares fit.

A. Sea and Lake Ice

Notes taken by an expert observer from Scott Polar Research Institute were used to categorize 187 samples from all UKMO flights, along with a qualitative assessment of ridging extent and snow cover. The following ice categories were observed: open water, grease ice, ice rind, light and dark nilas, rafted nilas, pancake ice, icecakes, close pack ice, compact consolidated ice, fast ice, lake ice, and arctic first-year ice.

The near-nadir emissivity was calculated for each category and is plotted in Fig. 2. A dotted line connects the spectra of each sample. Table III shows the average emissivity of each category and the fitted model parameters. These were used to calculate the solid lines shown in Fig. 2. The polarization-mixing parameter Q is estimated manually, as described in Section VI.

Open water included a range of sea states from 2 to 4 (2–8 m/s), observed in the Baltic and Arctic Seas, all close to 0°C. The continuous line compares these results with calculations based on recent permittivity measurements of sea water by Lamkaouchi *et al.* [22] at 0°C. The measurements at 24 and 50

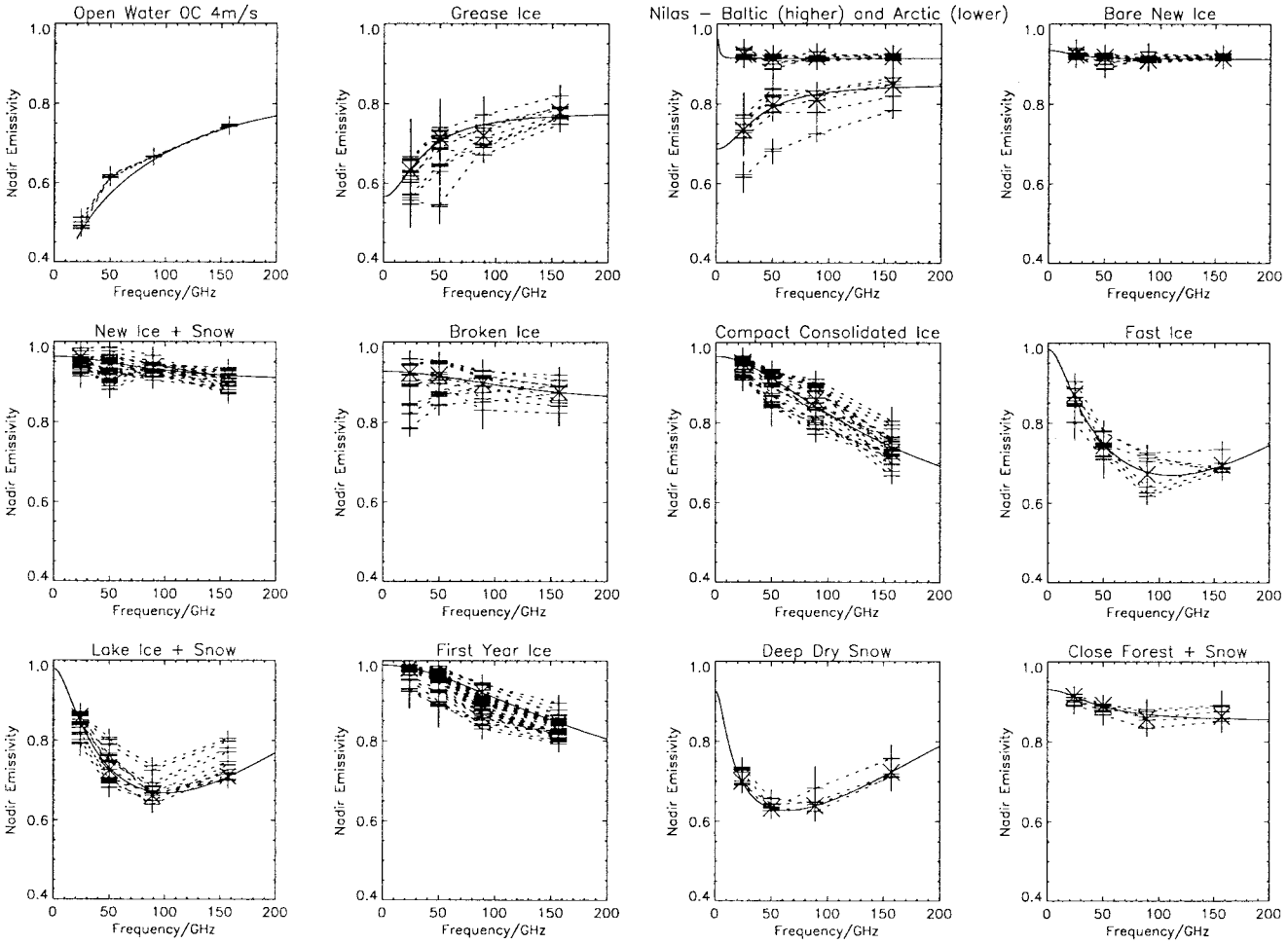

Fig. 2. Nadir emissivity spectra. All samples within each surface category are shown, linked with dashed lines, and error bars represent the standard error of mean. The fitted model is shown as a continuous line.

TABLE III
AVERAGE EMISSIVITY OF SURFACE CATEGORIES AND FITTED MODEL COEFFICIENTS

	Nadir emissivity				Permittivity Coeffs			Roughness	Pol.
Category	$\epsilon(24)$	$\epsilon(50)$	$\epsilon(89)$	$\epsilon(157)$	ε_s	ε_∞	ν_τ/GHz	σ/mm	Q
Water 0C	0.504	0.617	0.660	0.743	From [21]			0.0	0.00
Grease Ice	0.632	0.714	0.720	0.779	23.7	7.65	17.3	0.0	0.15
Baltic Nilas	0.924	0.916	0.918	0.919	1.60	3.34	2.18	0.0	0.00
Bare New Ice	0.923	0.918	0.910	0.915	2.86	3.40	27.0	0.0	0.00
New Ice + Snow	0.961	0.944	0.937	0.915	2.18	3.70	122	0.0	0.15
Broken Ice	0.923	0.918	0.897	0.875	3.03	5.47	183	0.0	N/A
Compact Pack ice	0.950	0.913	0.857	0.726	2.04	1.7e6	50e6	0.0	N/A
Fast Ice	0.872	0.744	0.672	0.696	1.66	77.8	703	0.1	0.35
Lake Ice + Snow	0.858	0.726	0.662	0.711	1.78	67.1	534	0.1	0.15
First Year Ice	0.981	0.964	0.922	0.844	1.52	84.5e3	4.7e6	0.0	N/A
Deep Dry Snow	0.700	0.633	0.640	0.724	3.02	24.0	59.9	0.1	0.15
Close Forest + snow	0.923	0.891	0.857	0.864	2.95	5.08	64.0	0.0	0.40
Fresh Wet Snow	0.957	0.962	0.964	0.955	2.22	109	45e3	0.0	N/A

GHz are consistently higher than this model, due to specular reflections of the aircraft contaminating Deimos' downward view. MARSS views 12° to the right of the aircraft, therefore avoiding reflections of the aircraft entering the field of view.

Grease ice is matt, brownish ice undulating as surface waves, but also includes flat, shiny ice rind. This category was thinner than 10 mm, and the emissivities showed a strong dependence on the thickness, ranging from those of open water to thick new ice.

Nilas includes light, dark, and rafted nilas, which could not be resolved radiometrically. This is flat, new ice with no air or brine pockets, and hence exhibits no significant surface or

volume scattering. Again, the emissivity is dependent on the ice thickness, saturating when it is greater than about 30 mm. The upper line represents a best fit calculated for only the thicker samples of Baltic nilas. This shows high emissivity across the spectrum, as expected. The limited amount of Arctic nilas observed generally has lower emissivity than that found in the Baltic due to the difference in salinity. The lower curve is a fit to only the Arctic samples, which may be thinner than the ice used to calculate the Baltic nilas line. As saturation was not observed in the spectra of Arctic nilas, these results should not be taken as definitive, and have thus been neglected from Table III.

Bare new ice is thicker, homogeneous, flat, dark ice formed within the last few days, undisturbed by pressure ridging or snowfall. It is characterized by a flat emissivity spectra. This excludes Arctic samples.

Snow-covered new ice is as above, but includes a thin cover (a few centimeters) of fresh, dry snow. This category also includes *pancake ice* (close-packed, regular, circular floes of less than 10 m diameter) and *icecakes* (similar, with larger diameter). Lower frequencies see a higher effective emissivity, as they penetrate the snow to the slightly warmer underlying surface. *Compact consolidated ice* measured on April 2, 1995, when the snow cover was wetter, is included in this category due to its spectral characteristics.

Broken ice covers a variety of forms, from pure slush found in fine-grained *Shuga, brash ice* to larger, crushed ice floes making up *close* and *very close pack ice.* This grouping shows a large range of spectra due to the irregularity of the samples' ice fields.

Compact consolidated ice comprises large ice floes that have frozen together, often with ridging and variable amounts of dry snow cover. This was the most extensive ice type observed in the Baltic during MACSI, and was typically 30–50 cm thick. The spectrum shows lower emissivity at higher frequencies, characteristic of the volume-scattering mechanism of small brine and air pockets within the thicker, older icepack and its snow cover. It should also be noted that this spectrum is very close to that of *multiyear ice* found in the literature [23].

Fast ice is the landlocked ice found along the northern shore of the Baltic. It is typically 60 cm thick, and has a flat surface as it cannot be affected by pressure ridging, and occasionally has a thin (a few centimeters) cover of snow. This is the oldest of the Baltic ice types (although still "first year"), and volume scattering is evident, even at 24 GHz. Some samples did show spectra intermediate between that of fast ice and other types. These are presumed to be transitional types, and are not included in this analysis. A trend is evident for an increase in emissivity above 100 GHz, which suggests increasing absorption, although scattering is still the dominant mechanism.

Lake ice + snow was observed near Pudasjärvi, between the snow test sites, and Jeesiö on March 15, 1997. The four higher samples on this plot were measured on April 2, 1995 when the snow cover was not completely dry ($T_s' \approx -2$°C), and were excluded from the fit calculation. Despite the snow cover, these areas showed very similar emissivity spectra to fast ice, which has a similar structure. This is evidence that brine pockets do not dominate the volume-scattering process. The consistent increase at 157 GHz suggests that higher frequencies are sensitive to a feature of the snow pack, such as absorption by a thin surface ice crust, which would be penetrated by lower frequencies. This is characteristic of many dry snow surfaces (see Section V-D), and is independent of surface temperature, over the observed range of -15 to -3°C.

Arctic first-year ice was measured near Svalbard on April 7, 1995. This shows an emissivity spectrum close to that of Baltic *compact consolidated ice* (which shares similar appearances), although less depressed at higher frequencies. Although small patches of blue–green colored ice were observed, suggesting the presence of multiyear ice, no significant sample could be measured, and reference to the ice chart showed the aircraft track to be well to the south of the multiyear ice [17].

B. Cloverleaf Over Ridged Ice

On April 5, 1995, the UKMO C-130 performed a "cloverleaf" pattern over heavily ridged, compact consolidated ice. This involved overflying the same area in eight directions to test for an emissivity dependence on view angle with respect to ridge orientation. No significant dependence on azimuth angle was observed in the emissivities averaged along 5 km legs. However, the ridging was not uniformly aligned on this scale, and variations on smaller scales may well be resolvable [24].

C. Dry Snow Over Land

The four snow sites observed in MACSI proved inhomogeneous, due to variable forestry cover, snow depth, and wetness. However, snow measured near Sodankylä was uniformly deep ($\approx$1 m) and dry ($T_s < -11$°C). This allowed the identification of homogeneous periods according to the solar albedo as measured by the aircraft's pyranometers. Only the lowest altitude runs (76 m) were used for this, to achieve the maximum resolution from the pyranometers. Four periods, totaling 90 s, were classified as "open snow," where the albedo was over 0.75. Video footage and GPS records were then checked to ensure that these were not lakes. Five further periods were identified as "close forest + snow," where the albedo was less than 0.25 and the canopy cover was 60% at nadir. Although the underlying surface was snow covered, the trees were generally snow free. The results are included with those from the ice categories in Fig. 2 and Table III.

Deep dry snow near Sodankylä also shows an increase in emissivity at 157 GHz. But in this case, the emissivity at 24 GHz is even lower than it was for lake ice. This is because volume scattering within the deeper snow pack is now having an effect at lower frequencies. However, if the snow pack were deeper still, and so its transmissivity became zero, the emissivity at 24 GHz would probably decrease further to the limit, representing the single-scattering albedo.

Close forest + snow is seen to have a higher emissivity, representing a 60 : 40 mix of dense forestry, with an emissivity of 1.00 [25] and "deep dry snow." Again, if the snow in the forest clearings were deeper, the emissivity at 24 GHz would be expected to decrease.

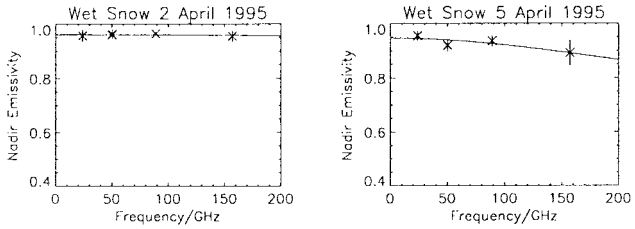

Fig. 3. Nadir emissivity spectrum for wet snow over land when fresh and after three days' freeze/thaw cycle. Error bars represent the standard deviation. Continuous lines show model fitted to data.

D. Wet Snow Over Land

Wet snow was observed during two MACSI flights at the low-lying snow sites, which included some forest cover. As homogeneous samples could not be identified, a different categorization scheme was adopted to extract the emissivity of wet snow from these data.

Areas where the solar albedo, measured by the aircraft hemispherical pyranometers, was greater than 0.6 were classified as open snow. Where this was coincident with a surface temperature greater than -2°C, as measured by the aircraft infrared radiometer, the snow was classified as wet as it is likely to have a significant fraction of liquid water present.

This classification scheme for wet snow was applied to all data measured at low level over land on April 2 and 5, 1995. The nadir emissivity spectrum of the selected data is shown in Fig. 3.

Fresh wet snow was found to have a high emissivity ($\epsilon \approx 0.96$) at all frequencies when fresh on April 2. Model coefficients based on a best fit of these data only are given in Table III. This behavior is expected due to the strong absorption by liquid water particles in the snow pack. However, after three days, the emissivity at 157 GHz has decreased, and has become more variable. This result suggests that this channel is sensitive to a metamorphosis of the snow grains near the surface as a result of the intervening freeze–thaw cycle.

E. Refrozen Snow Over Land

It was not possible to diagnose refrozen snow by the above scheme. Although it has somewhat lower albedo than fresh snow, it may be indistinguishable from fresh snow with partial vegetation cover.

The emissivity gradient $\Delta\epsilon = \epsilon(24\ \text{GHz}) - \epsilon(50\ \text{GHz})$ has been used to diagnose refrozen snow due to the Rayleigh reflectivity spectrum ($\Gamma \propto \nu^4$) of scattering by the large snow grains [27]. Histograms show the distribution of $\Delta\epsilon$ over the same area of land on April 2, 4, and 5, 1995 in Fig. 4. A consistent increase can be seen as the snowfall of April 1–2 ages due to the diurnal freeze–thaw cycle. Note also the smaller maxima at higher values of $\Delta\epsilon$, corresponding to measurements over lake ice. In reported refrozen snow spectra [26], it is expected that $\Delta\epsilon = +0.27$. No areas were found with $\Delta\epsilon$ as high as this. The largest such gradient observed (except over lake ice) was $+0.1$ on April 5, 1995. This is consistent with the findings of Mätzler [27] for snow covered with a refrozen crust a few centimeters thick, typical of the conditions experienced during MACSI.

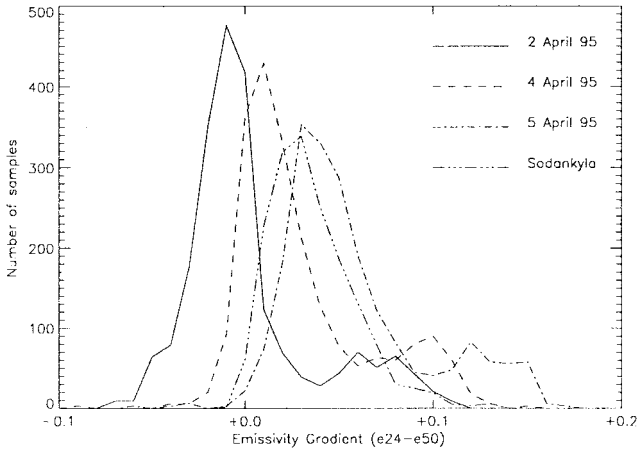

Fig. 4. Histograms of distribution of emissivity gradient ϵ(24 GHz $-$ ϵ(50 GHz) observed over snow-covered land.

VI. Emissivity Variation with Incidence Angle

In March 1997, Deimos was capable of measuring two polarizations. This allowed a useful investigation into the variation of emissivity with view angle and polarization, which can be compared with predictions of the proposed model.

Both of Deimos's channels measure two orthogonal polarizations in each of its five downward views. These polarizations rotate with scan angle, so as to align to "vertical" and "horizontal" in the forward view ($+35$°). However, there is evidence from measurements over open water [25] that the horizontal polarization of the 50 GHz channel is somewhat misaligned, causing the polarization contrast to be underestimated.

MARSS's channels measure only one polarization in each of its nine downward views. This polarization rotates with scan angle. The 157 GHz channel is aligned so the polarization rotates from "horizontal" in the $+20$° view to "vertical" in the -40° view. The polarization of the 89 GHz channel also rotates, but only approaches horizontal in the nadir view and is intermediate at the scan extremes.

The same samples used to calculate nadir emissivity were trimmed, by removing the first and last 3 s, to ensure that the scan extremes are not exposed to contrasting scenes. The emissivity was then calculated for each of the instruments' views.

Fig. 5 shows the mean and standard error of the emissivity measured in each view for the categories measured on March 15, 1997, together with lines fitted to the effective permittivity coefficients calculated in Table III, shown as solid lines for the V and H polarizations. The dashed lines show the average of these polarizations, calculated by setting the polarization-mixing parameter $Q = 0.5$.

Nilas and *bare new ice* show closely specular behavior at all frequencies. The polarization appears somewhat suppressed for *grease ice*, which is not perfectly flat, but undulates slightly. However, the large variance of this category, caused by different thicknesses of this grease ice, may also explain this.

The snow cover on new ice tends to decrease the polarization contrast due to volume scattering in the snow pack.

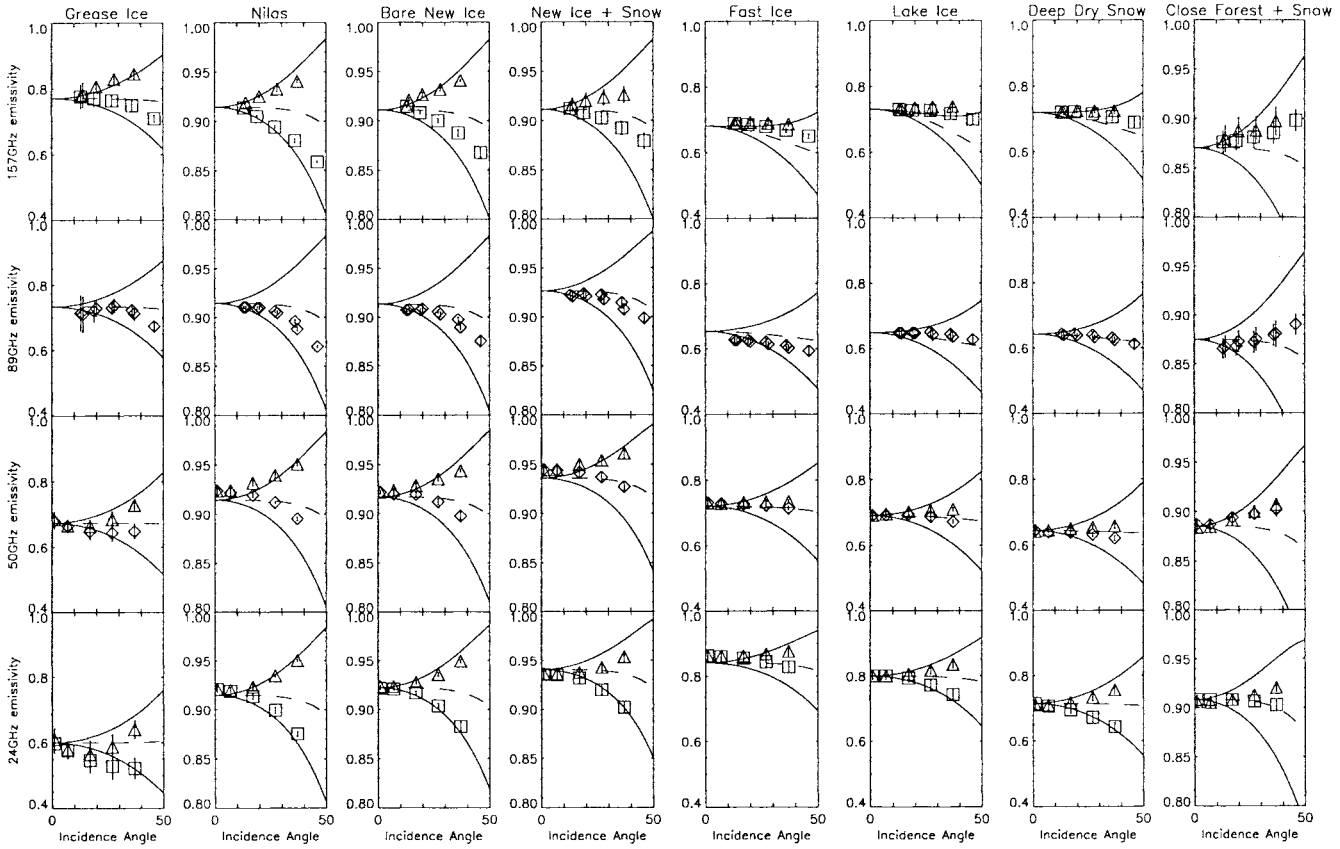

Fig. 5. Average emissivity of all samples within each surface category observed on March 15, 1997. Graphs are shown for all observed frequencies at all incidence angles. Symbols represent observed polarization: $\triangle$ = vertical, $\square$ = horizontal, $\diamond$ = intermediate. Continuous lines show predictions of model fitted in Section V for purely specular reflections of vertical and horizontal polarizations. Broken line shows the average of these ($Q = 0, 5$).

Snow also increases its apparent emissivity at 24 GHz, which penetrates the thin snow layer to view the warmer ice below.

Fast ice shows very little polarization contrast, except at 24 GHz, due to large-scale roughness, which could be modeled by geometric optics or more simply represented by setting $Q = 0.50$. Although *lake ice* has a similar nadir emissivity spectra to fast ice, it exhibits a much larger polarization contrast at low frequencies due to its smoother underlying surface.

Snow over land is usually thicker than that on lake ice, as it is less exposed to blowing winds. This is reflected by the lower emissivity at 24 and 50 GHz, as the snow pack is now thick enough (approximately 90 cm) to produce significant volume scattering at these lower frequencies. Again, the snow shows strong polarization at 24 GHz, decreasing with frequency.

Close forest with snow cover is characterized by very low polarization contrast and emissivity that increases at higher view angles. This is due to the changing geometry of the scene: the trees' height obscures more of the underlying snow surface when viewed obliquely.

The small residual polarization apparent at 157 GHz in the last four categories is believed to be an instrumental bias, as has also been observed in zenith views.

VII. Conclusions

A procedure has been developed to retrieve surface emissivity from airborne measurements of microwave and thermal infrared brightness temperatures, allowing for atmospheric contributions. This allowed emissivity spectra to be produced for eight categories of sea ice and three of snow-covered land, and gave results close to expected values over open water.

Results were close to those in the literature below 100 GHz. The emissivity of thick new ice is high, but decreases at higher frequencies in older ice. Snow cover decreases the emissivity of new ice at high frequencies, but has little effect on older ice types. Baltic compact consolidated ice was found to have similar characteristics to Arctic first-year ice, but Baltic nilas had a higher emissivity than that found in the arctic. Fast ice and snow-covered lake ice types also had similar spectra. Wet snow appears almost black when fresh, but its emissivity decreases at high frequencies as it ages.

The emissivity at 157 GHz was found to be anomalously high over strongly scattering surfaces, such as dry snow, lake, and fast ice. This channel's emissivity may be poorly predicted if the spectrum is assumed to be monotonic.

Further examination of the emissivity's variation with incidence angle showed new ice surfaces to behave in a specular way, whereas other surfaces were found to depolarize emissions due to surface scattering.

A semiempirical model has been developed, based on specular reflection and a Debye-like form of effective permittivity. This was shown to be capable of reproducing the measured emissivity spectra, with the addition of a Bragg scattering term to represent the nonmonotonic variation experienced in some

surface categories, especially at 157 GHz. Such a model can be used to provide a background emissivity for satellite retrievals over the snow and ice surface measured.

ACKNOWLEDGMENT

The authors wish to thank E. Attema for arranging ESA's funding of the MACSI flights and E. Aldworth for her expert observations of ice types. The authors acknowledge the support of the ground and air crew of the Royal Air Force, the scientists and technicians of the Meteorological Research Flight, especially R. Saunders, for all of their efforts during the MACSI experiment. S. O'Donnell, A. Kirkman, and T. Jukes are particularly thanked for their hard work in the development of the Deimos radiometer just in time for this experiment. The authors are particularly endebted to D. Jones for refining the instruments' calibration. C. Mätzler's comments were also appreciated.

REFERENCES

[1] S. J. English, "Ice and snow emission and scattering: Results from SAAMEX and proposals for the MACSI experiment," Met Office (RS) Branch Memo. 17; available from Y70 DERA, Farnborough, Hants. GU14 0LX, U.K., 1995.

[2] L. Tsang, J. A. Kon, and R. T. Shin, *Theory of Microwave Remote Sensing.* New York: Wiley (Series on Remote Sensing), 1985.

[3] F. T. Ulaby, R. K. Moore, and A. K. Fung, *Microwave Remote Sensing—Active and Passive, Volume I: Microwave Remote Sensing Fundamentals and Radiometry.* Reading, MA: Addison-Wesley, 1981.

[4] K. M. St. Germain, C. T. Swift, and T. C. Grenfell, "Determination of dielectric constant of young sea ice using microwave spectral radiometry," *J. Geophys. Res.,* vol. 98, no. C3, pp. 4675–4679, 1993.

[5] J. C. Maxwell-Garnett, "Colors in metal glasses and in metallic films," *Philos. Trans. R. Soc. Lond. A,* vol. 203, pp. 385–420, 1904.

[6] A. Stogryn, "A study of the microwave brightness temperature of snow from the point of view of strong fluctuation theory," *IEEE Trans. Geosci. Electron.,* vol. GE-24, pp. 220–231, Mar. 1986.

[7] A. W. Lohanick, "Microwave brightness temperatures of laboratory-grown undeformed first-year ice with an evolving snow cover," *J. Geophys. Res.,* vol. 98, no. C3, pp. 4667–4674, 1993.

[8] I. Sherjal, M. Fily, O. Grosjean, J. Lemorton, B. Lesaffre, Y. Page, and M. Gay, "Microwave Remote sensing of snow from a cable car at chomonix in the French Alps," *IEEE Trans. Geosci. Remote Sensing,* vol. 36, pp. 324–328, 1998.

[9] A. W. Lohanick and T. C. Grenfell, "Variations in brightness temperature over cold first year sea ice near Tuktoyaktuk, Northwest Territories," *J. Geophys. Res.,* vol. 98, no. C4, pp. 5133–5144, 1993.

[10] S. J. English, "Estimation of temperature and humidity profile information from microwave radiances over different surface types," *J. Appl. Meteorol.,* 1998, submitted for publication.

[11] B. J. Choudhury, T. J. Schmugge, A. Chang, and R. W. Newton, "Effect of surface roughness on the microwave emission from soils," *J. Geophys. Res.,* vol. 84, no. C9, pp. 5699–5706, 1979.

[12] J. R. Wang and B. J. Choudhury, "Remote sensing of soil moisture content over bare field at 1.4 GHz frequency," *J. Geophys. Res.,* vol. 86, pp. 5277–5282, 1981.

[13] T. Hewison, "The design of Deimos: A microwave radiometer with channels at 23.8 GHz and 50.3 GHz for the UK Met. research flight C-130 aircraft," in *Proc. IGARSS'95,* 1995, pp. 2261–2263.

[14] S. J. English, C. Guillou, C. Prigent, and D. C. Jones, "Aircraft measurements of water vapor continuum absorption," *Q. J. R. Meteorol. Soc.,* vol. 120, pp. 603–625, 1994.

[15] T. J. Hewison and S. J. English, "Analysis of a microwave airborne campaign over snow and ice (MACSI)," in *Proc. EMAC94/95 Final Results Workshop WPP-136,* ESTEC, 1997.

[16] T. J. Hewison, "MACSI data summary," Met Office(RS), Y70 DRA, Farnborough, Hants. GU14 0LX, U.K., Branch Working Paper 99, 1997.

[17] S. J. English, "MACSI flight summary for UK MRF Hercules," available from Met Office (RS), Y70 DRA, Farnborough, Hants. GU14 0LX, U.K., 1995.

[18] J. R. Eyre, "A fast radiative transfer model for satellite sounding systems," ECMWF Tech. Memo. 176.

[19] H. J. Liebe, "MPM—An atmospheric millimeter wave propagation model," *Int. J. Inf. Millim. Waves,* vol. 10, no. 6, pp. 631–650, 1989.

[20] A. Berk, L. S. Bernstein, and D. C. Robertson, "MODTRAN: A moderate resolution model for LOWTRAN7," Air Force Geophys. Lab., Hanscom AFB, MA, GL-TR-89-0122, 38 pp., 1989.

[21] J. W. Salisbury, D. M. D'Aria, and A. Wald, "Measurements of thermal infrared spectral reflectance of frost, snow and ice," *J. Geophys. Res.,* vol. 99, no. B12, pp. 24235–24240, 1994.

[22] K. Lamkaouchi, A. Balana, and W. J. Ellison, "New permittivity data for Sea Water (30–100 GHz)," Rep. on extension to ESTEC/ESA Contract 11197/94/NL/CN, 1996.

[23] M. A. Janssen, *Atmospheric Remote Sensing by Microwave Radiometery.* New York: Wiley (Series on Remote Sensing), 1993, p. 318.

[24] L. D. Farmer, D. T. Eppler, and A. W. Lohanick, "Passive microwave signatures of fractures and ridges in sea ice at 33.6 GHz (vertical polarization) as observed in aircraft images," *J. Geophys. Res.,* vol. 98, no. C3, pp. 4645–4665, 1993.

[25] T. J. Hewison, "Airborne measurements of NOPEX forest and agricultural land surface microwave emissivity," Met Office (RS) Branch Mem. 21, Met Office (RS), Y70 DERA, Farnborough, Hants. GU14 0LX, U.K., 1998.

[26] N. C. Grody, "Surface identification using satellite microwave radiometers," *IEEE Trans. Geosci. Remote Sensing,* vol. 26, pp. 850–859, Nov. 1988.

[27] C. Mätzler, "Passive microwave signatures of landscapes in winter," *Meteorol. Atmos. Phys.,* vol. 54, pp. 241–260, 1994.

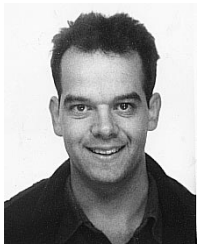

Tim J. Hewison (M'97) received the B.Sc. (Hons.) degree in physics with astrophysics from the University of Manchester, U.K., in 1989.

Since 1990, he has been with the Remote Sensing Branch of the U.K. Meteorological Office. His work has included the analysis of AMSU-B radiometric and antenna tests, and the development of the new microwave radiometer ("Deimos") for the U.K. Meteorological Office C-130 research aircraft. He is now involved in the planning and analysis of aircraft experiments to measure the microwave emissivity of various surface types.

Stephen J. English received the B.Sc. degree in physics and meteorology from the University of Reading in 1988, and the D.Phil. degree in 1991 from the University of Oxford, concentrating on the use of passive microwave observations for retrieving meteorological parameters.

From 1992 to 1995, he worked for the Remote Sensing Branch of the U.K. Meteorological Office, where he used data from an airborne microwave radiometer to test microwave emission and absorption models. In 1995, he became Head of the Satellite Sounding Group at the U.K. Meteorological Office, contributing to the move toward assimilation of TOVS radiances into the numerical weather prediction model using a variational framework.